Colloids and Surfaces B: Biointerfaces 220 (2022) 112939

Contents lists available at ScienceDirect

Colloids and Surfaces B: Biointerfaces

journal homepage: www.elsevier.com/locate/colsurfb

Structuring and de-structuring of nanovectors from algal lipids. Part 1: physico-chemical characterization

I. Clemente [a,e,*], F. D'Aria [b], C. Giancola [b], C. Bonechi [a,e], M. Slouf [c], E. Pavlova [c], C. Rossi [a,e], S. Ristori [d,e]

[a] Department of Biotechnology, Chemistry and Pharmacy, University of Siena, via A. Moro 2, Siena 53100, Italy
[b] Department of Pharmacy, University of Naples Federico II, via D. Montesano 49, Napoli 80131, Italy
[c] Institute of Macromolecular Chemistry, Academy of Sciences of the Czech Republic, Heyrovského nám. 2, 162 06 Prague, Czech Republic
[d] Department of Chemistry "Ugo Schiff", University of Florence, via della Lastruccia 3, 50019 Sesto Fiorentino, FI, Italy
[e] Center for Colloid and Surface Science (CSGI), via della Lastruccia 3, 50019 Sesto Fiorentino, FI, Italy

ARTICLE INFO

Keywords:
Nanocarriers
Algal lipids
Structure
Morphology
Molecular interactions

ABSTRACT

Lipid nanocarriers are among the most employed systems for drug delivery purposes in several research and industrial sectors, since their favorable properties ensure broad applicability. The design and characterization of these nanosystems are of paramount importance to obtain controlled outcome, since the supramolecular structure and molecular interactions deeply impact the functionality of the resulting aggregates. The choice of the most appropriate formulation for the target of interest relies on in-depth physico-chemical characterization in order to optimize stability, loading rates and sustained release. Several supramolecular architectures suited for carrier development can be obtained from lipid building blocks, by varying lipid composition and packing parameter. In particular, cubosome and liposome aggregates are often used as drug vectors thanks to their high cargo capability and biocompatibility. Moreover, the possibility to employ lipids from natural sources i.e. biomasses to prepare nanosystems makes them especially attractive. In this work, two aggregate types were characterized and compared as drug vectors for poorly water-soluble antioxidants, particularly curcumin and two adjuvants (i.e. tocopherol and piperine). The nanovectors were obtained by extracting lipids from algal biomasses with different lipid composition, and characterized by advanced structural (DLS, SAXS, Cryo-TEM) techniques, spectroscopy (NMR) and calorimetry (ITC). Finally, the structural stability of both aggregate types was evaluated.

1. Introduction

Lipid-based aggregates of various symmetries have reached remarkable popularity in the field of drug delivery [1–3]. Even though these systems can differ greatly in supramolecular architecture and functional properties, all possess suitable characteristics for nanocarrier development. Generally, lipid nanosystems present good biocompatibility and biodegradability, easiness of preparation due to their spontaneous self-assembly, and favourable encapsulation capability [4,5]. However, the design and preparation of efficient formulations for drug delivery involves (i) the study of the structural properties at different length scales and (ii) the optimization of cargo loading, stability and sustained release [1,4]. The structural analysis concerns both the organization of the lipid phase and the interaction with guest molecules, to unravel the parameters influencing the carrier mechanism of action, while the study of drug loading, stability and release involves testing in various media which simulate biomimetic environments [6–8].

Lipid bicontinuous cubic phases are nonlamellar mesophases formed in concentrated solutions by amphiphilic molecules with both positive and negative curvature at the lipid-water interface, leading to self-assembly in three-dimensional structures where the surface is draped around two non-interconnected water channels [9–11]. These aggregates are topologically described by the theory of infinitely periodic minimal surfaces, where every surface point is a saddle point with zero mean curvature [12,13]. The three main known geometries of cubic phases (Pn3m double-diamond, Im3m primitive and Ia3d gyroid) are defined by their crystallographic group [1,4,9]. The more common lipid lamellar phases are formed by molecules with packing parameter close

* Corresponding author at: Department of Biotechnology, Chemistry and Pharmacy, University of Siena, via A. Moro 2, Siena 53100, Italy.
E-mail address: ilaria.clemente2@unisi.it (I. Clemente).

https://doi.org/10.1016/j.colsurfb.2022.112939
Received 25 May 2022; Received in revised form 13 September 2022; Accepted 13 October 2022
Available online 14 October 2022

to unity, which leads to their arrangement into planar bilayers. In dilute conditions these latter can close to form vesicles with various degree of lamellarity, though the most used are the unilamellar assemblies [3,4]. Both cubic and unilamellar nanosystems are popular in drug delivery [14] and can be found in biological processes and entities [12,15]. Many characterization techniques have been used to investigate these systems, their interactions with guest molecules and functionality as delivery agents. High-resolution structural techniques, such as Small Angle X- ray Scattering (SAXS) and Cryo-Transmission Electron Microscopy (cryo-TEM) are generally the most appropriate to obtain in-depth knowledge of supramolecular architecture [16,17]. The interactions of the carrier with guest molecules can be investigated by calorimetry, such as Isothermal Titration Calorimetry (ITC) that gives thermodynamic data or by spectroscopy such as Nuclear Magnetic Resonance (NMR), that provides information on structure and dynamics at molecular level.

The analysis of the nanovectors loading and stability to evaluate drug delivery efficacy is generally carried out in biomimetic media, with various degrees of complexity [18]. This characterization involves the use of nonspecific solutions at a certain pH, temperature and salt concentration, and sometimes organic solvents, to assess the impact of these conditions on vector stability and cargo bioaccessibility [19–22]. In particular, hydroalcoholic solutions have been used to simulate accelerate destructuring conditions in months-long studies, or simply harsher environments to test stability. The results thus obtained have shown high correlation with experiments conducted in standard media [23,24].

Following previous work in our laboratory [25], herein we present the investigation and comparison of two series of lipid nanovectors, cubosomes and liposomes, built with lipids extracted from the dried biomass of the microalga *Nannochloropsis* sp. This microorganism is able to accumulate different lipid classes depending on the culture media [26,27]. Specifically, two biomasses with different lipid composition were used in this work, one with prevalence of phospholipids and other polar lipids and the second mainly made of triglycerides, which form preferentially lamellar and nonlamellar (cubic) aggregates, respectively. The design and preparation procedure involving natural sources grants the possibility to obtain biocompatible dispersed nanosystems through a sustainable approach [26,28,29]. These nanocarriers were loaded with a well-known poorly water-soluble antioxidant, i.e. curcumin, alone or together with tocopherol or piperine as adjuvants, to achieve slow release and high bioaccessibility. The obtained formulations were investigated and compared from the perspective of supramolecular aggregation by Dynamic Light Scattering (DLS), synchrotron SAXS and Cryo-TEM, while the interactions between carrier and guest molecules were studied by NMR and ITC. Finally, the stability and release properties at bulk level were tested in biorelevant conditions, namely both media with physiological surfactants and then with progressively higher percentages of ethanol, to simulate release in harsh conditions of bilayer perturbation. Indeed, previous experiments carried out with water dilution and/or abrupt pH or ionic force variations had showed that the nanocarriers studied herein were highly resistant in these conditions. Thus, increasingly hostile media were simulated to study de-structuring at molecular and supramolecular level. This combination of techniques allowed to obtain a multiscale perspective on the systems structuring and stability and to perform preliminary assessments of their applicability.

2. Materials and methods

2.1. Reagents

All solvents and compounds were bought from Sigma-Aldrich and used as received. The Regenerated Cellulose (RC) Spectra/Por dyalisis membranes were bought from SpectrumLabs.com. The algal biomasses of *Nannochloropsis oceanica* F&M-M24 from the Fotosintetica & Microbiologica (F&M) S.r.l. culture collection were cultivated outdoors at F&M facility (Florence, Italy) and characterized as previously described (see Supporting Information, Table S1) [26,27,30]. The biorelevant medium was purchased from Biorelevant.com Ltd, UK.

2.2. Sample preparation

The two lyophilized and powdered algal biomasses were stored in freezer at − 20 ± 1 °C and de-frozen before use to prevent degradation, then lipid extraction was performed in Folch solution ($CHCl_3/CH_3OH$ 2:1 v/v) by weighing 25 mg/mL for samples with lower concentration, and 40 mg/mL for samples loaded at higher concentration, which were employed for SAXS studies. The solutions were stirred for 24 h at room temperature, then the solvents were evaporated to obtain a lipid film. Stock solutions of the three antioxidants in acetone were added to the dry film in the appropriate concentrations. Subsequent evaporation was performed under vacuum to obtain a dry lipid film, which was then rehydrated using MilliQ water and equilibrated for 12 h. The obtained suspensions were subjected to extensive vortexing followed by eight freeze-and-thaw cycles. Finally, high-power sonication using a Bandelin Sonopuls HD 4050 probe sonicator (frequency 20 kHz) was employed to downsize the lipid nanovectors, as previously described [26]. Two series of systems were studied in this work, namely cubosomes and liposomes. The composition of each sample with loaded antioxydants is reported in Table 1.

2.3. Dynamic light scattering

DLS measurements were performed on a Malvern Zetasizer (Nano ZS) equipped with a He–Ne 633 nm, 4 mW laser and backscattering optics, after diluting the samples 1:200 with MilliQ water to adjust optical turbidity. The cumulant expansion was employed to analyze the autocorrelation function of the scattered intensity and to obtain mean size and polydispersity index, employing the instrument software. All measurements were recorded in triplicate (n = 3) and averaged, then standard deviation was calculated with OriginPro software.

2.4. Small angle X-ray scattering

SAXS experiments were performed at the high-brilliance ID02 beamline of the European Synchrotron (Grenoble, France) [31]. The wavelength of the incoming beam was 1 Å, and the sample-to-detector distances were 0.8, 10, and 31 m covering a total q range of 3×10^{-3} to 7.5 nm^{-1} ($q = (4\pi/\lambda)\sin\theta$, where 2θ is the scattering angle and q the

Table 1
Sample list, loaded compounds and concentrations.

Sample name	Supramolecular structure	Loaded compound	Loaded concentration
Empty-cub	cubosome	–	–
C1-cub	cubosome	Curcumin (C)	10^{-2} M
CT-cub	cubosome	C+ α-tocopherol (T)	10^{-2} M (C), 5×10^{-3} M (T)
CP-cub	cubosome	C+ piperine (P)	10^{-2} M (C), 5×10^{-3} M (P)
C2.5-cub	cubosome	Curcumin (C)	2.5×10^{-2} M
C2.5 T-cub	cubosome	C+ α-tocopherol (T)	2.5×10^{-2} M (C), 1.25×10^{-2} M (T)
C2.5 P-cub	cubosome	C+ piperine (P)	2.5×10^{-2} M (C), 1.25×10^{-2} M (P)
Empty-lip	liposome	–	–
C1-lip	liposome	Curcumin (C)	10^{-2} M
CT -lip	liposome	C+ α-tocopherol (T)	10^{-2} M (C), 5×10^{-3} M (T)
CP -lip	liposome	C+ piperine (P)	10^{-2} M (C), 5×10^{-3} M (P)
C2.5 -lip	liposome	Curcumin (C)	2.5×10^{-2} M
C2.5 T-lip	liposome	C+ α-tocopherol (T)	2.5×10^{-2} M (C), 1.25×10^{-2} M (T)
C2.5 P-lip	liposome	C+ piperine (P)	2.5×10^{-2} M (C), 1.25×10^{-2} M (P)

momentum transfer). The 2D SAXS patterns initially recorded were azimuthally averaged to obtain 1D patterns and normalized to the absolute scale with a standard procedure reported elsewhere [32]. The sample holder was a flow-through capillary of 2 mm diameter.

2.5. Cryogenic transmission electron microscopy

Cryo-TEM experiments were performed on a Tecnai G2 Spirit Twin microscope (FEI, Czech Republic) at the Polymer Morphology department of the Institute of Macromolecular Chemistry (Czech Academy of Sciences, Prague). The microscope was equipped with a cryo-attachment (Gatan, USA). For cryogenic microscopy 3 μl of sample solution were dropped on electron microscopy grid covered with a holey carbon supporting film (Electron Microscopy Sciences/Mir Biotech, Czech Republic), which was hydrophilized just before the experiment by glow discharge (Expanded Plasma Cleaner, Harrick Plasma, USA). The excess solution was removed by blotting (Whatman no. 1 filter paper) for 1 s, and the grid was plunged into liquid ethane at −181 °C. The frozen samples were kept at liquid nitrogen temperature (−196 °C), inserted in the cryo-holder and transferred into the microscope. TEM observations were performed at −173 °C using bright field imaging at 120 kV accelerating voltage.

2.6. Nuclear magnetic resonance

NMR spectra were recorded on Bruker 600 spectrometer (DRX-600 AVANCE), operating at 14.07 T and equipped with an *xyz* gradient unit, at 298 K. Monodimensional ^{1}H experiments were acquired with 128 scans over 64 K of data, a spectral width of 6000 Hz and relaxation delay of 5s. A resolution enhancement function (LB=0.5 Hz) was applied before Fourier transformation. The spectra were processed using the Bruker TOPSPIN 3.5 Software. All samples were prepared employing D_2O.

2.7. Isothermal titration calorimetry

ITC measurements were performed using a nano-ITC (TA instruments, USA) at 25 °C. Water or hydroalcoholic solution were injected (syringe volume 50 μl) into the calorimetric vessel (170 μl) containing a lipid dispersion (Empty-lip, Empty-cub, C1-lip and C1-cub 0.5 mM), in aliquots of 2 μl with 300s interval. The dilution heat was evaluated in control experiments by injecting water or hydroalcoholic solution into the water alone or with ethanol 10 % or 30 % v/v. Moreover, the interactions between loaded liposomes or cubosomes were evaluated by injecting P-lip or P-cub and T-lip or T-cub (1.7 mM) into the calorimetric vessel containing C1-lip or C1-cub (0.5 mM), in aliquots of 2 μl with 600s intervals. The heat produced by the dilution was evaluated in control experiments by injecting the nanovectors in water. For all experiments, the heat flow values were plotted versus time after correction for dilution heat. All measurements were performed in duplicate or triplicate, and the error associated to the Heat Flow is below 5 %.

2.8. Absorption spectroscopy

Encapsulation efficiency (EE %) was quantified by UV–Vis. The samples were properly diluted in ethanol to disrupt the nanovectors and release the entrapped molecules, as previously reported [23]. Absorption spectra were recorded at room temperature on a Thermo Scientific Evolution 220 UV–Vis spectrophotometer, equipped with a xenon flash lamp and double-beam geometry, using 10 mm path length quartz cuvettes. Absorption maxima at 425 nm, 350 nm and 270 nm were chosen for curcumin, piperine and α-tocopherol, respectively. The quantification was carried out recording the absorbances of standard solutions in dynamic range of linearity (curcumin 0.92–3.68 mg/L; α-tocopherol, 2.15–8.6 mg/L; piperine, 0.285–2.85 mg/L) and calibration curves showing correlation factors $R^2 > 0.990$ were accepted for subsequent analyses. All spectra were recorded in triplicate and averaged (n = 3). The EE % of nanovectors was calculated as follows:

$$Encapsulation\quad efficiency\quad (\%) = \frac{loaded\quad amount}{tot\quad amount} * 100 \tag{1}$$

For stability and release tests in hydroalcoholic solutions the samples were analyzed at final dilution of 1:500, in the linearity range of curcumin and at 425 nm. The baseline for UV-Vis measurements was measured with control hydroalcoholic solution at the correspondent percentage. The cumulative release values were calculated from the calibration curve using equation (2) and normalizing samples with their previously measured EE % [26].

$$Cumulative\quad release\quad (\%) = \frac{Abs\quad sample}{Abs\quad Std} * 100 \tag{2}$$

2.9. Stability and release experiments in biorelevant media

Stability and release experiments were performed in a Simulated Gastric Fluid (SGF) (Biorelevant.com Ltd, UK) [33] containing physiological surfactants and salts at pH ~2.5, mixed with increasing ethanol concentrations (40 % to 60 % v/v in increments of 10), to simulate progressively more hostile conditions and evaluate the release profile in this environment. Samples were diluted 1:2.5 and 1 mL was introduced in a previously re-hydrated 6–8 kD RC dialysis membrane, that was then submerged in 200 mL of release medium at 37 °C under stirring [7]. Then 500 μl aliquots were taken from the external medium every 2 h in triplicate and replaced with fresh medium kept in the same state to maintain sink conditions for 48 h. This time interval was chosen to monitor release for a sufficient time and avoid excessive presence of curcumin in the release medium and consequent degradation.

The same experimental setup (choosing only hydroalcoholic solution 60 % v/v) was employed to carry out the investigation of de-structuring at supramolecular level by synchrotron SAXS of both nanovector series (see SI). Sample aliquots (20 μl) were taken from inside the dialysis bag every 2 h and diluted to a sufficient volume for SAXS analysis (200 μl).

3. Results and discussion

3.1. Dynamic light scattering

The size distribution analysis in Dynamic Light Scattering showed that both liposome and cubosome series contained two polydisperse populations, indicating coexistence of aggregates with different sizes. Such data were in agreement with previous results [26] on cubosomes and showed similar profile of dimensions also for liposomes. Even though the complexity of the starting lipid mixtures resulted in some polydispersity that affected the results, DLS measurements established that samples in the same nanovector series had a similar range of aggregate size (Table 2, Figure S1). Specifically, both series showed a

Table 2
Size distribution values, standard deviation, populations ratio and polydispersity index (PdI) for all investigated samples. OriginPro software was used for data analysis.

Sample name	Mean size (nm) Peak 1 ± SD	Mean size (nm) Peak 2 ± SD	Populations ratio (Peak1/Peak2)	PdI
Empty-cub	48 ± 3	404 ± 35	0.010	0.3
C1-cub	153 ± 15	663 ± 68	0.066	0.45
CT-cub	69 ± 8	494 ± 43	0.011	0.3
CP-cub	59 ± 2	376 ± 78	0.011	0.35
Empty-lip	133 ± 20	2168 ± 68	0.017	0.4
C1-lip	318 ± 32	548 ± 50		0.43
CT -lip	–	495 ± 51	–	0.27
CP -lip	148 ± 37	550 ± 220	0.080	0.5

small population (Peak 1) with mean hydrodynamic diameter generally below 100 nm for cubosomes and above 100 nm for liposomes; a second population (Peak 2) at higher values around 500 nm was identified in all samples, showing good enough reproducibility in repeated measures. Values obtained above the nanometer scale likely accounted for the presence of impurities of the biomass. The samples loaded with guest molecules often presented bigger dimensions, but not dramatically so, with respect to empty samples, showing the ability of the nanocarriers to adjust their molecular arrangement to accommodate the cargo. This last evidence was more noticeable taking into account peak 1 in particular, that was considered more reliable than the second, more affected by artifacts due to impurities.

3.2. Small angle X-ray scattering

Two different concentrations of lipids and loaded molecules were used to prepare the nanovectors for SAXS analysis. In these samples the lipid/guest molecule ratio was fixed in order to investigate the influence of both lipid and antioxidant total content on the aggregation and ordering at supramolecular level. This effect was compared in liposomes and cubosomes to evidence their distinct behavior.

Figure S2 shows an exemplificative comparison between two liposome samples, Empty-lip and C1-lip and the correspondent cubosome samples Empty-cub and C1-cub, all at lower lipid and guest molecule concentration (Table 1). For both types of systems, the indexing of Bragg peaks was established and the positions typical of lipid ordering are evidenced by colored bars and labelling in figure (Fig. 1, Figure S2). In the case of cubosomes two coexisting cubic symmetries were identified, the Pn3m and the Im3m [9,11,34], clearly superposed to a background ascribable to the large bumps of form factors The form factor also governed the scattering intensity profile of liposomes, where only sample C1-lip showed the presence of slightly pronounced peaks identifying lamellar organization (green numbers in Figure S2), superposed to the form factor typical of bilayers. This is consistent with the SAXS profile of diluted regimes. Moreover, it could also be noticed the presence in both Empty-cub and C1-cub samples of three peaks (green labels in Figure S2) aligned with smaller peaks in sample C1-lip, which identify the 1:2:3… spacing of a lamellar stacking. When the samples were prepared at higher lipid and guest molecule concentrations, a peculiar behavior was evidenced in the two series, in that while liposomes showed no visible enhancement of the lipid ordering (Figure S3), cubosomes showed the appearance of sharper peaks (Fig. 1 evidenced by bars and indices, Figure S4) for both the coexisting cubic symmetries. This indicated a marked influence of curcumin on the overall ordering of cubosomes, in accordance with previous results [26]. Indeed, curcumin incorporation was able to impart tighter packing of cubic aggregates and more structured supramolecular organization [35].

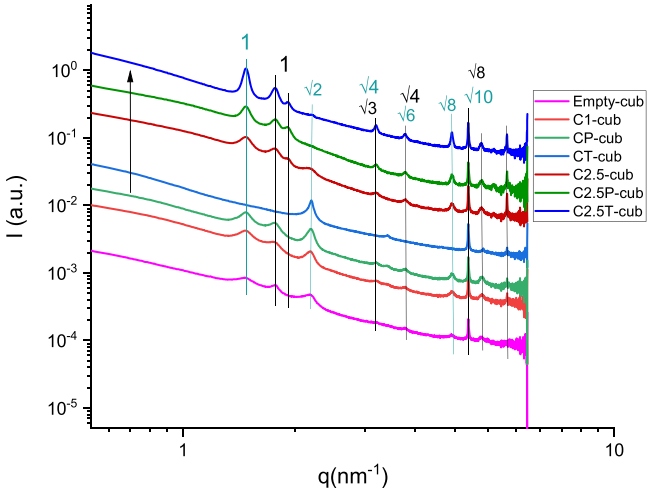

Fig. 1. One-dimensional SAXS intensity plot showing the positions of Bragg peaks in the two cubic mesophases (cyan and black labels indicating the q-spacing) for cubosome samples at the two lipid and guest molecule concentrations. The lattice parameter for the two phases, calculated according to the literature [36], is equal to 4.5 nm for Im3m phase and 3.8 nm for Pn3m phase.

SAXS was also employed to assess the de-structuring and progressive loss of supramolecular organization during stability tests in biorelevant medium mixed with hydroalcoholic solution (see Figures S5-S6). The scattering plots of both liposomes and cubosomes evidenced the gradual structure loosening over time, although both aggregate types showed remarkable stability and resistance to disassembling. Indeed, even though the ordering evidenced by the Bragg peaks was lost in the spectrum of the first aliquot (recorded after two hours), the form factors were still visible in both aggregate types (Figures S5-S6).

3.3. Cryogenic transmission electron microscopy

Typical cryo-TEM micrographs of cubosomes and liposomes are displayed in Fig. 2. The visualization of individual aggregates in cryo-TEM was carried out after establishing an optimal protocol for sample vitrification. All TEM specimens contained rather thick layers, that could be attributed to the natural material present in the samples, that enveloped the nanosystems which in turn tended to adhere to each other and form bigger aggregates. Nevertheless, within the high number of micrographs showing this large and thick aggregates, we could identify isolated particles: in cubosomes (Table 1, first four rows of Table 2; Fig. 2A) the particles were more compact (higher contrast in TEM micrographs), slightly smaller (mostly below 100 nm) and slightly irregular in shape, whereas in liposomes (Table1 and the last four rows of Table 2; Fig. 2B) the particles were larger (mostly above 100 nm), almost ideally spherical, and sometimes with onion-like structures (Fig. 2B; two-shell onion nanoaggregate in the center of the micrograph). The morphological differences between individual samples within given group (i.e. within the cubosome and liposome set of samples, respectively) were negligible. Nevertheless, it is fair to note that Fig. 2 shows typical isolated particles for both series, but the particle size distribution was broad in both cases. This is evidenced in Fig. 2: cubosomes contained also bigger particles (Fig. 2C), while liposomes contained also smaller particles (Fig. 2D). Moreover, some micrographs (Figure S7) documented that liposomes contained also very small metastable aggregates. The fact that particle size distributions of all investigated systems were quite complex, but the average size of liposomes was higher in comparison with cubosomes, corresponded well with DLS results (cf. Fig. 2 with Table 2).

3.4. Nuclear magnetic resonance

In lyotropic systems molecules experience different motions and averaging of anisotropic interactions depending on their long range symmetry [38]. Systems with cubic lipid structures can be differentiated from liposomes thanks to their motionally averaged NMR spectra [37,38]. Indeed, the lateral diffusion in onion-like lamellar systems does not change the molecular angle with the applied magnetic field, whereas in cubic phases the translational diffusion on the curved surface of the supramolecular aggregate results in additional averaging of dipolar interactions and new relaxation pathways, causing marked line narrowing [39]. Moreover, the fast translational diffusion in the isotropic structure of cubic systems modulates all inter- and intramolecular interactions. Thus, cubic phases are characterized by narrow, micellar-like, NMR signals. Contrarily, lamellar phases do not experience diffusion along planes and show instead relaxation by slower motions which results in broad spectra.

The NMR investigation of our diluted systems (liposomes and cubosomes) complied with the above-described peculiarities of lamellar and cubic phases respectively, both regarding lipid supramolecular

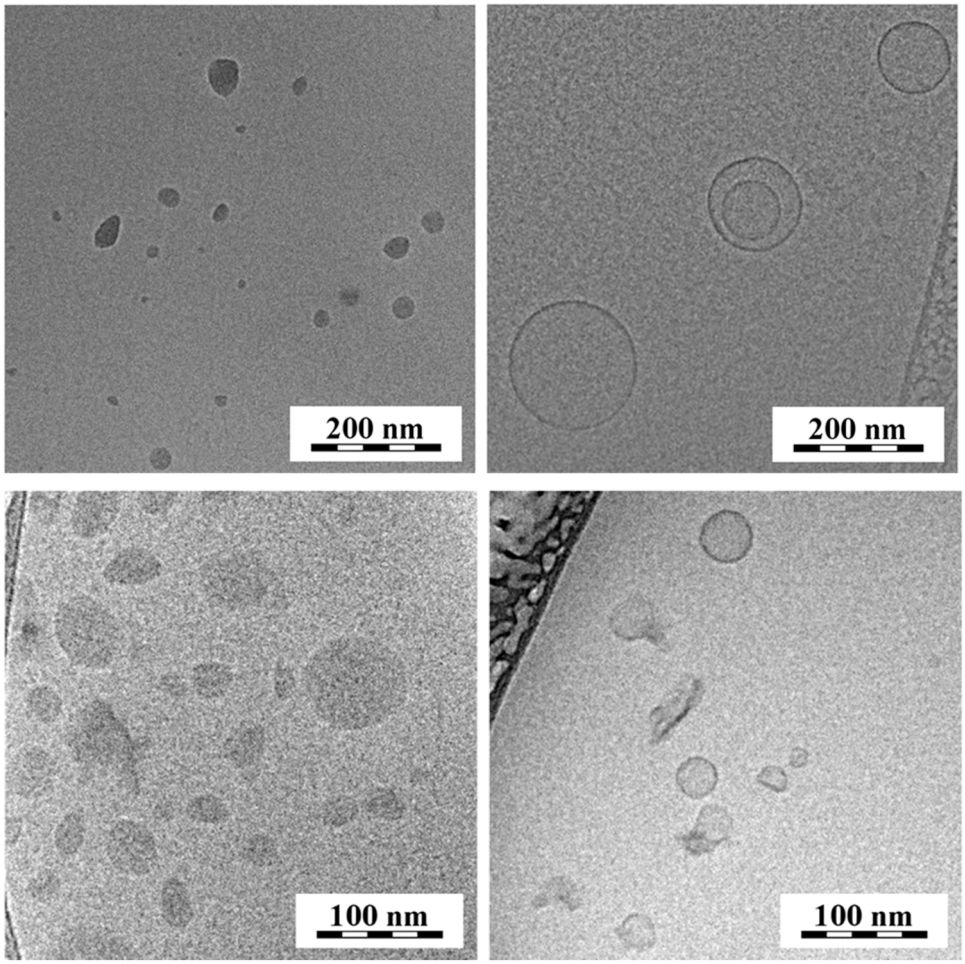

Fig. 2. Representative cryo-TEM micrographs from a) to d) left to right and top to bottom respectively, showing nanoaggregates in cubosomes (left, a and c) and liposomes (right, b and d). Micrographs c-d evidenced broad particle size distributions within the samples, namely that (c) cubosome systems contained also bigger aggregates and (d) liposome systems contained also smaller aggregates, as indicated by DLS.

structure and guest molecule incorporation. As shown in Fig. 3, the comparison of the ^{1}H spectra of Empty-cub (black curve) and Empty-lip (red curve) clearly evidenced the different packing and aggregation of the two nanovectors types. Indeed, the proton signals of the lipid matrix in the liposome sample were rather broad in the range 5–5.5 ppm, where protons experiencing intermediate de-shielding (e. g. protons close to the polar heads or bound to unsaturated carbons) resonate. Such tendency could be identified also in the range at 3–4 ppm, accounting for the terminal -CH_3 and -CH_2 groups in the alkyl chains. These findings were indicative of tight packing in liposomes, oppositely to cubosomes that in both spectral ranges presented narrower signals.

Moreover, as shown in the ^{1}H spectra in Figure S8, when varied curcumin concentrations were encapsulated in liposomes, no detectable change of peak broadness was evident in the spectra, in contrast with the previously observed peak narrowing in cubosomes [26]. These data were in agreement with SAXS spectra, clearly showing that structural differences between the two aggregate series (Figure S3 and S4) had a deep impact on the motions of lipid molecules. Indeed, higher curcumin payload was able to induce closer molecular packing and structuring in cubosomes, confirming a different mobility and dynamics in the two series of nanovectors.

3.5. Isothermal titration calorimetry

The investigation of the interactions and stability of the two nanocarrier series was performed by ITC to complement structural knowledge with a thermodynamic approach. The data obtained from SAXS and NMR supported the hypothesis of a different influence exerted by guest molecules-lipid matrix interactions at molecular level, depending both on cargo and supramolecular arrangement. Considering the high sensitivity of nanocalorimetry, titration experiments were carried out either in water or hydroalcoholic solutions at low ethanol content (10 % and 30 % v/v) to reveal differences in the nanocarrier stability and probe the strength of intra-aggregate interactions. The results obtained with water dilution (see Figure S9 in SI) showed different thermal profiles according both to aggregate type and guest molecules. Though all samples showed low heat intensity, molecular fluctuations and intra-bilayer rearrangements were evidenced in sample C1-cub, which presented a markedly different behavior showing thermal events that occurred upon titration with water. This result suggested the presence of looser surface packing in cubosomes and easier rearrangement capability.

Experiments carried out by titration with ethanol 10 % v/v showed more complex profiles, which was expected since ethanol is able to intercalate more deeply than water in lipid bilayers. Fig. 4 shows the thermal profiles of samples Empty-cub and Empty-lip (top) and samples C1-cub and C1-lip (bottom) upon hydroalcoholic dilution with ethanol 10 % v/v. In this case it can be evidenced that both Empty samples showed thermal events (more intense for Empty-cub), likely undergoing small rearrangements at the bilayer level, while both C1-cub and C1-lip showed different profiles. It can be hypothesized that curcumin loaded nanocarriers experienced different destabilization due to the presence of

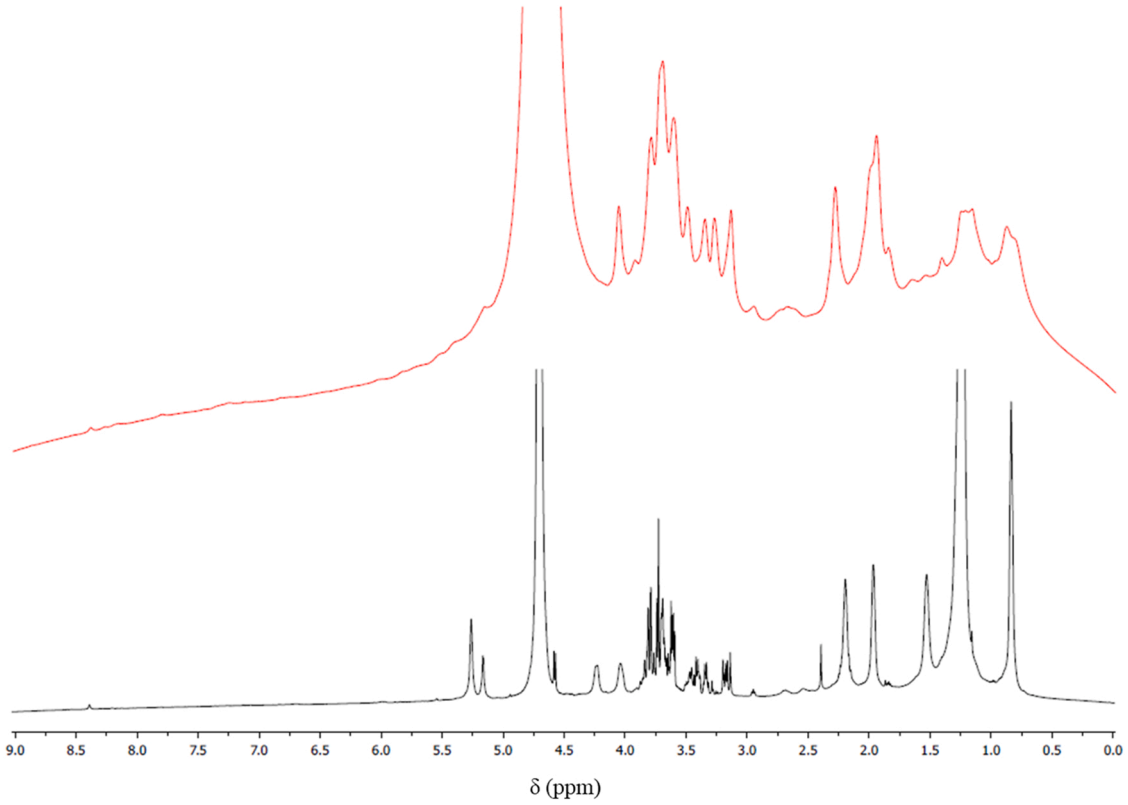

Fig. 3. ^{1}H NMR spectra of Empty-lip (red spectrum) and Empty-cub (black spectrum) recorded at 600 MHz and 298 K.

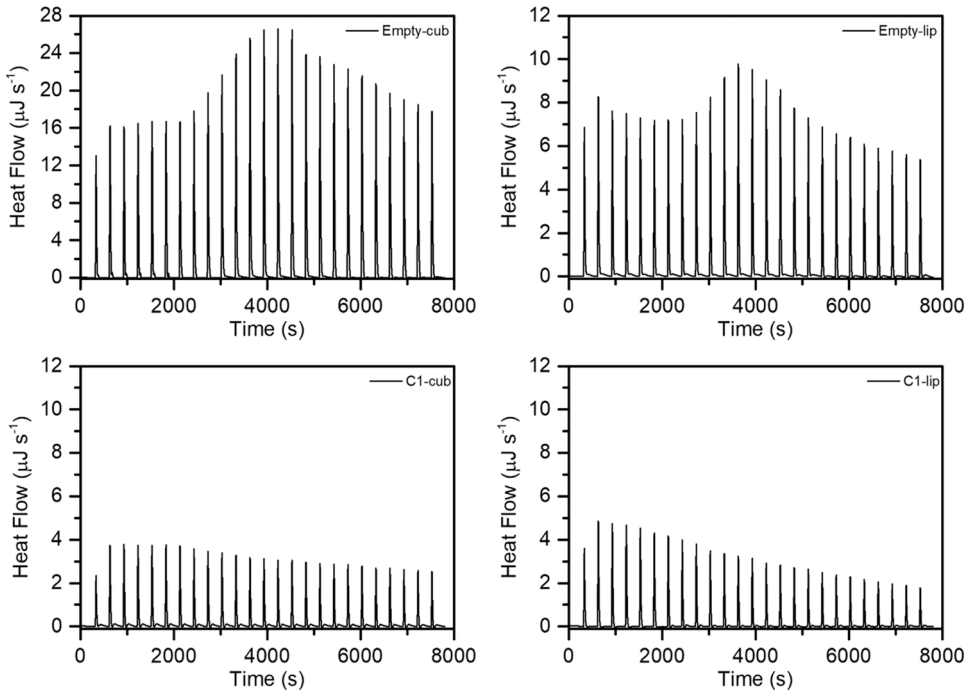

Fig. 4. Heat profiles of representative cubosome (Empty-cub and C1-cub, left column, top to bottom) and liposome samples (Empty-lip and C1-lip, right column, top to bottom) upon titration with ethanol 10 % v/v.

the guest molecule, that impacted differently on the lipid matrix structure with respect to empty aggregates. In the same way, all samples titrated with hydroalcoholic solutions with ethanol 30 % v/v (see Figure S10) underwent different thermal events upon bilayer destabilization, according to supramolecular structure and guest molecules. Overall, the hydroalcoholic titration resulted in a markedly active role of ethanol in the disassembly and rearrangement of the bilayer structures, tough higher percentages were needed to observe this effect on the supramolecular structure at macroscopic level, as discussed below (see discussion of spectrophotometric data).

A different titration modality, namely by diluting either C1-cub or C1-lip respectively with cubosomes or liposomes loaded with either tocopherol or piperine, was employed to investigate potential cargo-cargo interactions occurring in the confined bilayer space upon membrane fusion. In this case the thermal events concurring to the heat profiles depended on both carrier-carrier and cargo-cargo interactions. Fig. 5 shows that while liposome profiles suggested no bilayer rearrangement, the results obtained for cubosome samples confirmed a tendency for easier interaction and surface fusion. As suggested by the results of titrations with water (see Figure S9), this different behavior could be ascribed to looser density in the molecular packing on the surface of cubosomes, which led to more marked rearrangement capability. Moreover, the interaction between C1-cub and T-cub was associated to higher heat exchange, suggesting stronger affinity.

3.6. Encapsulation efficiency

The efficiency of guest molecule encapsulation in the nanosystems was assessed spectrophotometrically. The two aggregate types were compared to evidence the different encapsulation capability based on their structural arrangement in a structure-function perspective. Table S2 shows an opposite tendency in curcumin incorporation. Indeed, in cubosomes higher values of EE % were observed when tocopherol or piperine were loaded together with curcumin, as both adjuvants likely favored curcumin insertion thanks to interactions in the confined space of the lipid bilayer. Contrarily, liposomes showed the opposite trend, since samples CT-lip and CP-lip had lower EE % for curcumin than C1-lip (Table S2). Moreover, CT-cub and CP-cub showed higher curcumin encapsulation than CT-lip and CP-lip (Table S2). This could be explained considering the supramolecular arrangement, since the liposomal bilayer likely had lower encapsulation limit and could not adapt as easily as the cubic arrangement to accommodate the two molecules. Nevertheless, both nanocarrier series showed good encapsulation capability.

3.7. Stability and release experiments in biorelevant media/ethanol

The overall stability of lipid aggregates was tested firstly by using different methods to disrupt the vector-cargo association, such as dilution and abrupt pH or ionic force variation. These experiments revealed high resistance of the supramolecular structure to commonly used de-structuring techniques, since no release was detected in the medium at the bulk level, in contrast to the observed rearrangements at the molecular level. Moreover, control DLS measurements performed after these tests confirmed that the samples maintained their global size. Thus for both series the evaluation of stability and release profile under progressively harsher conditions was carried out by ethanol addition, to mimic a generic aggressive medium. Indeed, previous studies in the literature reported the use of organic solvents to accelerate destabilization and release [24,25]. Here, ethanol was selected for such evaluation both at molecular and bulk level due to its known ability to intercalate deeply in lipid bilayers and thus induce a disrupting effect on lipid packing. The structural study at different times in the destabilization was performed by SAXS. Figures S5-S6 show an exemplificative curve series reporting the time evolution of the scattering intensity, evidencing the progressive loss of structure with increasing time. In particular, increased broadening with final disappearance of Bragg peaks and loss of scattering intensity was always recorded as the systems disassembled and released their cargo. The latter effect could be evidenced and followed by Visible spectroscopy. Indeed, UV-Vis absorbance values measured at 425 nm resulted in similar release curves for all samples, where variations depended mostly on the encapsulated molecules rather than the nanovectors structure. Fig. 6 shows that both liposome and cubosome nanocarriers loaded with curcumin alone underwent similar fate. In general, all systems presented a three-steps pattern of destabilization and de-structuring, that eventually led to cargo release. Specifically, an initial burst followed by a linear trend and, finally, by a plateau was invariably observed. Regarding the ethanol content (Fig. 6A-6B), there was always a tendency going from a slow and sustained release at 40 % ethanol to a progressively more linear release in the first 6 h, and a plateau in 24 h at 60 %. Cubosomes showed a more regular trend, whereas liposomes presented an abrupt change from 40 % to 50 % ethanol (Fig. 6B). These results could be explained considering the nonspecific type of disruption conditions and the different re-arranging and self-assembly ability of the two supramolecular structures.

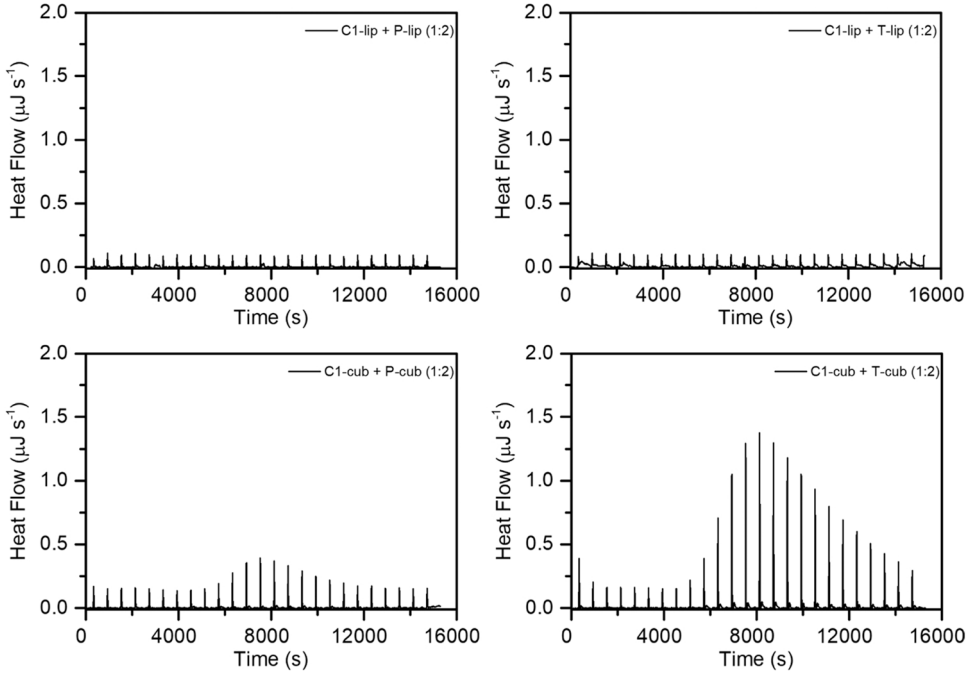

Fig. 5. Heat profiles of C1-lip sample titrated with either P-lip (1:2) or T-lip (1:2) (top, left to right) and C1-cub sample titrated with either P-cub (1:2) or T-cub (1:2) (bottom, left to right).

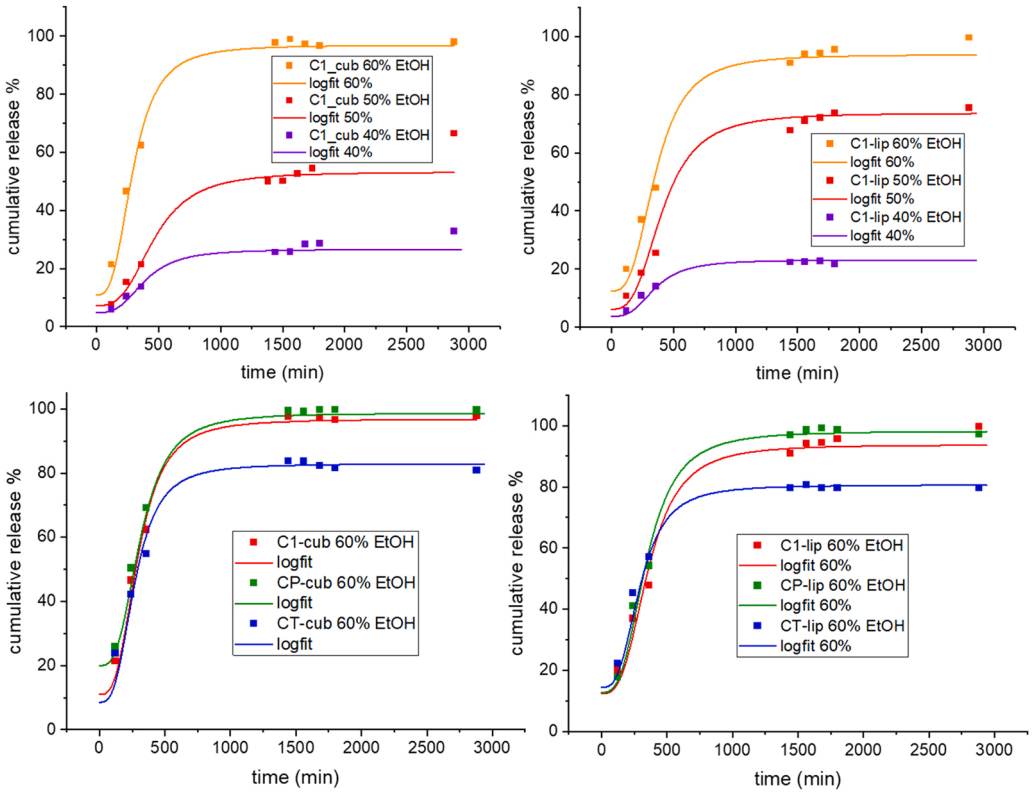

Fig. 6. (A-D). Top line: cumulative release profiles of C1-cub (A) and C1-lip (B) going from 40–60 % v/v hydroalcoholic solutions; bottom line: cumulative release profiles comparison of cubosome (C) and liposome (D) series at hydroalcoholic solution 60 % v/v.

Regarding comparisons among guest molecules, the cubosome series (Fig. 6C) showed higher release for CP-cub and slightly lower for C1-cub, whereas CT-cub showed markedly lower release values. A similar trend was observed also for liposomes (Fig. 6D) where CP-lip and C1-lip showed higher release values, whereas lower values were found for CT-lip. Such results evidenced the different role of the loaded molecules and their combined effect in the intercorrelation and structuring properties of the nanovectors. This finding was in agreement with SAXS results, once again evidencing the role played by guest molecules in the structuring and consequent stability of the nanocarriers, both at molecular and supramolecular scale.

4. Conclusions

In this work, two series of lipid nanoaggregates obtained from natural sources were designed and characterized. The biomass composition with prevalence of either polar or neutral lipids determined the assembly in distinct supramolecular architectures, showing lamellar or cubic symmetries. The obtained diluted nanocarriers were two series of liposomes and cubosomes, respectively. These systems were loaded with three hydrophobic antioxidants and their structural organization, morphology and interaction properties were investigated at molecular and supramolecular level. This multiscale perspective from complementary techniques allowed to characterize the resulting overall architectures, while the study of guest molecules-carrier interactions revealed a different influence of the cargo on bilayer packing density and intercorrelation. Particularly, the ability of curcumin to impose tighter structuring in cubosome bilayers was evidenced. The carrier stability and cargo-cargo interactions were also studied from molecular and macroscopic perspectives. High resistance at bulk scale and rearrangement capability at bilayer level in both nanocarrier types was showed by addition of ethanol, a typical bilayer intercalator and disrupter, here mimicking a non-specific interference agent. Cubosomes showed more pronounced capability for surface fusion and rearrangement, also according to loaded cargo, highlighting the relevance of both structure and cargo toward stability. In conclusion, the use of complementary physicochemical techniques allowed to obtain a comprehensive knowledge of the investigated formulations.

CRediT authorship contribution statement

Ilaria Clemente: Data curation; Formal analysis; Investigation; Methodology; Validation; Visualization; Writing – original draft; Writing – review & editing; **Federica D'Aria**: Data curation; Formal analysis; Investigation; Methodology; Visualization; Writing – original draft; Writing – review & editing. **Concetta Giancola**: Conceptualization; Resources; Supervision; Validation; Writing – review & editing. **Claudia Bonechi**: Data curation; Formal analysis; Investigation; Validation; Visualization; Writing – original draft. **Miroslav Slouf**: Data curation; Resources; Supervision; Visualization; Validation; Writing – original draft. **Ewa Pavlova**: Data curation; Formal analysis; Validation; Visualization; Writing – original draft. **Claudio Rossi**: Conceptualization; Funding acquisition; Project administration; Resources; Supervision; Validation; Writing – review & editing. **Sandra Ristori**: Conceptualization; Funding acquisition; Methodology; Project administration; Resources; Supervision; Validation; Writing – original draft; Writing – review & editing.

Declaration of Competing Interest

The authors declare that they have no known competing financial interests or personal relationships that could have appeared to influence the work reported in this paper.

Data availability

Data will be made available on request.

Acknowledgements

I.C. gratefully acknowledges MESOFARMA S.r.l. (Reggio Calabria, Italy) for funding her Ph.D. grant. The ID02 beamline staff, and in particular Dr. Theyencheri Narayanan and Dr. Michael Sztucki of the ESRF (Grenoble, France) are acknowledged for beamtime allocation and scientific support. Prof. Mario Tredici and Prof. Liliana Rodolfi from the Department of Agriculture, Food, Environment and Forestry (DAGRI), University of Florence are acknowledged for cultivation and analysis of the algal biomasses.

Appendix A. Supporting information

Supplementary data associated with this article can be found in the online version at doi:10.1016/j.colsurfb.2022.112939.

References

[1] J. Zhai, C. Fong, N. Tran, C.J. Drummond, Non-lamellar lyotropic liquid crystalline lipid nanoparticles for the next generation of nanomedicine, ACS Nano 13 (6) (2019) 6178–6206.
[2] A. Angelova, V.M. Garamus, B. Angelov, Z. Tian, Y. Li, A. Zou, Advances in structural design of lipid-based nanoparticle carriers for delivery of macromolecular drugs, phytochemicals and anti-tumor agents, Adv. Colloid Interface Sci. 249 (2017) 331–345.
[3] A. Akbarzadeh, R. Rezaei-Sadabady, S. Davaran, et al., Liposome: classification, preparation, and applications, Nanoscale Res Lett. 8 (2013) 102.
[4] A. Zabara, R. Mezzenga, Controlling molecular transport and sustained drug release in lipid-based liquid crystalline mesophases, J. Control Release 188 (2014) 31–43.
[5] L. Boge, H. Bysell, L. Ringstad, D. Wennman, A. Umerska, V. Cassisa, J. Eriksson, M.L. Joly-Guillou, K. Edwards, M. Andersson, Lipid-based liquid crystals as carriers for antimicrobial peptides: phase behavior and antimicrobial effect, Langmuir 32 (2016) 4217–4228.
[6] A. Angelova, M. Drechsler, V.M. Garamus, B. Angelov, Liquid crystalline nanostructures as PEGylated reservoirs of omega-3 polyunsaturated fatty acids: structural insights toward delivery formulations against neurodegenerative disorders, ACS Omega 3 (3) (2018) 3235–3247.
[7] C.V. Kulkarni, V.K. Vishwapathi, A. Quarshie, Z. Moinuddin, J. Page, P. Kendrekar, S.S. Mashele, Self-assembled lipid cubic phase and cubosomes for the delivery of aspirin as a model drug, Langmuir 33 (2017) 9907–9915.
[8] L. Tavano, R. Muzzalupo, N. Picci, B. de Cindio, Co-encapsulation of antioxidants into niosomal carriers: Gastrointestinal release studies for nutraceutical applications, Colloids Surf. B: Biointerfaces 114 (2014) 82–88.
[9] V. Luzzati, P. Mariani, T. Gulik-Krzywicki, The Cubic Phases of Liquid-Containing Systems: Physical Structure and Biological Implications in Physics of Amphiphilic Layers (1987) 131–137.
[10] K. Larsson, Cubic lipid-water phases: structure and biomembrane aspects, J. Phys. Chem. 93 (1989) 7304–7314.
[11] S. Aleandri, R. Mezzenga, The physics of lipidic mesophase delivery systems, Phys. Today 73 (2020) 38.
[12] S.T. Hyde, S. Andersson, K. Larsson, Z. Blum, T. Landh, S. Lidin, B.W. Ninham, The language of shape. The Role of Curvature in Condensed Matter: Physics, Chemistry and Biology, Elsevier, Amsterdam, 1997.
[13] S.T. Hyde, S. Andersson, A cubic structure consisting of a lipid bilayer forming an infinite periodic minimum surface of the gyroid type in the glycerolmonooleat-water system, Z. Krist. Cryst. Mater. 168 (1984) 213–220.
[14] C. Chang, T.G. Meikle, C.J. Drummond, Y. Yang, C.E. Conn, Comparison of cubosomes and liposomes for the encapsulation and delivery of curcumin, Soft Matter 17 (2021) 3306–3313.
[15] J. Kraineva, C. Nicolini, P. Thiyagarajan, E. Kondrashkina, R. Winter, Incorporation of α-chymotrypsin into the 3D channels of bicontinuous cubic lipid mesophases, Biochim. Et. Biophys. Acta 1764 (2006) 424–433.
[16] A. Angelova, B. Angelov, M. Drechsler, T. Bizien, Y.E. Gorshkova, Y. Deng, Plasmalogen-based liquid crystalline multiphase structures involving docosapentaenoyl derivatives inspired by biological cubic membranes, Front. Cell Dev. Biol. 9 (2021), 617984.
[17] N. Koifman, Y. Talmon, Cryogenic electron microscopy methodologies as analytical tools for the study of self-assembled pharmaceutics, Pharmaceutics 13 (2021) 1015.
[18] L. Zou, B. Zheng, R. Zhang, Z. Zhang, W. Liu, C. Liu, H. Xiao, D.J. McClements, Food-grade nanoparticles for encapsulation, protection and delivery of curcumin: comparison of lipid, protein, and phospholipid nanoparticles under simulated gastrointestinal conditions, RSC Adv. 6 (2016) 3126.
[19] L. Dai, Y. Wei, C. Sun, L. Mao, D.J. McClements, Y. Gao, Development of protein-polysaccharide-surfactant ternary complex particles as delivery vehicles for curcumin, Food Hydrocoll. 85 (2018) 75–85.
[20] F. Cuomo, M. Cofelice, F. Venditti, A. Ceglie, M. Miguel, B. Lindman, F. Lopez, In-vitro digestion of curcumin loaded chitosan-coated liposomes, Colloids Surf. B: Biointerfaces 168 (2018) 29–34.
[21] Y. Liu, D. Liu, L. Zhu, Q. Gan, X. Le, Temperature-dependent structure stability and in vitro release of chitosan-coated curcumin liposome, Food Res. Int. 74 (2015) 97–105.
[22] S. Chen, Q. Li, D.J. McClements, Y. Han, L. Dai, L. Mao, Y. Gao, Co-delivery of curcumin and piperine in zein-carrageenan core-shell nanoparticles: formation, structure, stability and in vitro gastrointestinal digestion, Food Hydrocoll. 99 (2020), 105334.
[23] M. Kamberi, S. Nayak, K. Myo-Min, T.P. Carter, L. Hancock, D. Feder, A novel accelerated in vitro release method for biodegradable coating of drug eluting stents: Insight to the drug release mechanisms, Eur. J. Pharm. Sci. 37 (2009) 217–222.
[24] D.R. Janagam, L. Wang, S. Ananthula, J.R. Johnson, T.L. Lowe, An accelerated release study to evaluate long-acting contraceptive levonorgestrel-containing in situ forming depot systems, Pharmaceutics 8 (2016) 28.
[25] I. Clemente, C. Bonechi, L. Rodolfi, M. Bacia-Verloop, C. Rossi, S. Ristori, Lipids from algal biomass provide new (nonlamellar) nanovectors with high carrier potentiality for natural antioxidants, Eur. J. Pharm. Biopharm. 158 (2021) 410–416.
[26] P. Bondioli, L. Della Bella, G. Rivolta, G. Chini Zittelli, N. Bassi, L. Rodolfi, D. Casini, M. Prussi, D. Chiaramonti, M.R. Tredici, Oil production by the marine microalgae Nannochloropsis sp. F&M-M24 and tetraselmis Suecica F&M-M33, Bioresour. Technol. 114 (2012) 567–572.
[27] L. Rodolfi, G. Chini Zittelli, N. Bassi, G. Padovani, N. Biondi, G. Bonini, M. R. Tredici, Microalgae for oil: strain selection, induction of lipid synthesis and outdoor mass cultivation in a low-cost photobioreactor, Biotechnol. Bioeng. 102 (2009) 100–112.
[28] I. Colzi, A.N. Troyan, B. Perito, E. Casalone, R. Romoli, G. Pieraccini, N. Škalko-Basnet, A. Adessi, F. Rossi, C. Gonnelli, S. Ristori, Antibiotic delivery by liposomes from prokaryotic microorganisms: similia cum similis works better, Eur. J. Pharm. Biopharm. 94 (2015) 411–418.
[29] I. Clemente, F. Menicucci, I. Colzi, L. Sbraci, C. Benelli, C. Giordano, C. Gonnelli, S. Ristori, R. Petruccelli, Unconventional and sustainable nanovectors for phytohormone delivery: Insights on *Olea europaea*, ACS Sus Chem. Eng. 6 (2018) 15022–15031.
[30] F. Menicucci, M. Michelozzi, A. Raio, M. Tredici, G. Cencetti, I. Clemente, S. Ristori, Thymol-loaded lipid nanovectors from the marine microalga Nannochloropsis sp. as potential antibacterial agents, Biocatal. Agric. Biotechnol. 32 (2021), 101962.
[31] T. Narayanan, M. Sztucki, P. Van Vaerenbergh, J. Leonardon, J. Gorini, L. Claustre, F. Sever, J. Morse, P. Boesecke, A multipurpose instrument for time-resolved ultra-small-angle and coherent X-ray scattering, J. Appl. Cryst. 51 (2018) 1511–1524.
[32] P. Boesecke, Reduction of two-dimensional small- and wide-angle X-ray scattering data, J. Appl. Crystallogr 40 (2007) 423–427.
[33] Biorelevant.com
[34] C. Fong, T. Le, C.J. Drummond, Lyotropic liquid crystal engineering–ordered nanostructured small molecule amphiphile self-assembly materials by design, Chem. Soc. Rev. 41 (2012) 1297.
[35] Z.Y. Ng, J.-Y. Wong, J. Panneerselvam, T. Madheswaran, P. Kumar, A. Hsu, N. Hansbro, M. Bebawy, P. Wark, P. Hansbro, K. Dua, D.K. Chellappan, Assessing the potential of liposomesloaded with curcumin as a therapeutic intervention in asthma, Coll. Surf. B: Biointerfaces 172 (2018) 51–59.
[36] A. Tilley, Y.-D. Dong, H. Amenitsch, M. Rappolt, B.J. Boyd, Transfer of lipid and phase reorganisation in self-assembled liquid crystal nanostructured particles based on phytantriol, Phys. Chem. Chem. Phys. 13 (8) (2011) 3026.
[37] J. Charvolin, P. Rigny, Proton relaxation study of paraffinic chain motions in a lyotropic liquid crystal, J. Chem. Phys. 58 (1973) 3999.
[38] T.G. Meikle, D.W. Keizer, J.J. Babon, C.J. Drummond, F. Separovic, C.E. Conn, S. Yao, Physiochemical characterization and stability of lipidic cubic phases by solution NMR, Langmuir 36 (22) (2020) 6254–6260.
[39] D.D. Lasic, Magnetic resonance methods in the studies of liposomes, Bull. Magn. Reson. 13 (1991) 3–13.